ADVANCES IN ATMOSPHERIC SCIENCES, VOL. 33, FEBRUARY 2016, 233–246

The Impact of Deformation on Vortex Development in a Baroclinic Moist Atmosphere

Na LI[1], Lingkun RAN*[1], and Shouting GAO[1,2]

[1]*Key Laboratory of Cloud-Precipitation Physics and Severe Storms, Institute of Atmospheric Physics, Chinese Academy of Sciences, Beijing* 100029

[2]*State Key Laboratory of Severe Weather, Chinese Academy of Meteorological Sciences, Beijing* 100081

(Received 24 March 2015; revised 7 July 2015; accepted 26 July 2015)

ABSTRACT

A mathematical relation between deformation and vertical vorticity tendency is built by introducing the frontogenesis function and the complete vertical vorticity equation, which is derived by virtue of moist potential vorticity. From the mathematical relation, it is shown that properly configured atmospheric conditions can make deformation exert a positive contribution to vortex development at rates comparable to other favorable factors. The effect of deformation on vortex development is not only related to the deformation itself, but also depends on the current thermodynamic and dynamic structures of the atmosphere, such as the convective stability, moist baroclinicity and vertical wind shear (or horizontal vorticity). A diagnostic study of a heavy-rainfall case that occurred during 20–22 July 2012 shows that deformation has the most remarkable effect on the increase in vertical vorticity during the rapid development stage of the low vortex during its whole life cycle. This feature is mainly due to the existence of an approximate neutral layer (about 700 hPa) in the atmosphere where the convective stability tends to be zero. The neutral layer makes the effect of deformation on the vertical vorticity increase significantly during the vortex development stage, and thus drives the vertical vorticity to increase.

Key words: deformation, low vortex, vorticity, frontogenesis function

Citation: Li, N., L. K. Ran, and S. T. Gao, 2016: The impact of deformation on vortex development in a baroclinic moist atmosphere. *Adv. Atmos. Sci.*, **33**(2), 233–246, doi: 10.1007/s00376-015-5082-y.

1. Introduction

In meteorology, deformation is mostly applied to the frontogenesis process (Petterssen, 1956; Yang et al., 2014; Yang et al., 2015). However, many observations and a number of clear and simple theories show that deformation also plays important roles in other physical processes, such as storm-track dynamics, the formation and maintenance of the moat structure in tropical cyclones, symmetric instability, blocking onset, and so on (e.g., Whitaker and Dole, 1995; Elhmaidi et al., 2004; Rivière and Joly, 2006a, b; Gao et al., 2008; Wang, 2008; Thomas, 2012; Moon and Nolan, 2015). Based on the traditional exponential growth problem of normal modes (Charney, 1947; Eady, 1949; Kuo, 1949), Farrell (1989) demonstrated that, although the deformational flow does not support any exponentially growing solution, disturbance embedded in the deformational flow undergoes transient development. Mak and Cai (1989) obtained a general condition for the stability property of a perturbation embedded in a non-divergent 2D barotropic flow, stated as: "to optimally extract (kinetic) energy from the basic flow, a perturbation must be elongated locally along the axis of contraction of the basic deformation field" [physically interpreted by Cai (1992)]. In addition, Cai and Mak (1990) derived a whole set of energy equations for local perturbations in a zonally inhomogeneous baroclinic jet streak in a two-layer quasi-geostrophic beta-plane channel model [Cai and Mak, 1990, Eqs. (10–13)]. With these equations, Mak (1991) verified the "eddy straining" mechanism proposed by Shutts (1983), which argues that due to the impact of deformation, the transient eddy stretches along the north–south direction and compresses in the zonal direction, causing transformation of momentum and energy to the blocking flow and stimulating the blocking onset. Apart from discussing the perturbation growth mode within the deformation field, Weiss (1991) obtained a condition for the vorticity gradient increasing (Okubo–Weiss condition), to explain the vortex filament phenomenon with the conserved vertical vorticity equation in a barotropic and non-divergent atmosphere. According to the condition, the vertical vorticity gradient increases when the strength of the deformation square is larger than the vorticity square, and changes periodically when the vorticity square is larger than the deformation square. This theory has been used to explain the mechanism of the moat structure in tropical cyclones (Rozoff et al., 2006; Wang, 2008). These studies

* Corresponding author: Lingkun RAN
Email: rlk@mail.iap.ac.cn

© Institute of Atmospheric Physics/Chinese Academy of Sciences, and Science Press and Springer-Verlag Berlin Heidelberg 2016

demonstrate well that deformation may play important roles in the physics of some weather phenomena, as emphasized by Spensberger and Spengler (2014), who stated that deformation may be used as a diagnostic tool in large-scale processes, e.g., low-level frontogenesis, evolution of high-level jets, orographic blocking, and Rossby wave breaking.

While most of the above research is associated with the deformation of a barotropic atmosphere, some investigators have focused on the relation between deformation and disturbances in a baroclinic atmosphere. Bishop and Thorpe (1994a, 1994b) indicated that deformation has key effects on the unstable development of frontal waves, but may simultaneously suppress these waves. Renfrew et al. (1997) also argued that the magnitude of stretching deformation of the environmental flow (Bishop, 1996a, 1996b) is crucial to the frontal stability. Wang and Wu (2001) found that a symmetric disturbance tends to develop under the ascending flow of the transverse circulation caused by deformational frontogenesis. With a 2D shallow-water model, Jiang (2011) investigated the formation and evolution of meso-β-scale low vortexes embedded in the deformational flow. In addition, Jiang et al. (2011) proposed an interaction index between vortex and deformation flow, which was shown to be able to indicate the short-term direction of movement of a tropical cyclone. These investigations have provided significant insight into vortex development in a baroclinic atmosphere, implying an important role of deformation in baroclinic vortex evolution. However, most of these results were obtained from idealized numerical experiments, which are not easy to use in diagnostic analyses of the real atmosphere. For a barotropic atmosphere, both the non-divergent perturbation kinetic energy equation (Mak and Cai, 1989) and the Okubo–Weiss condition (Weiss, 1991) can be used to diagnose the possible roles of deformation in disturbance development. However, in a baroclinic atmosphere, a quantitative description and diagnosis of the impact of deformation on vortex development remains unrealized.

Therefore, in this paper, a mathematical relation between deformation and the vertical vorticity tendency is built to describe and diagnose the impact of deformation on mesoscale low vortices in a baroclinic atmosphere. The corresponding formulation is presented in section 2. With this mathematical relation, a diagnostic study of the impact of deformation on vortex development in a heavy-rainfall case is reported in section 3. Finally, section 4 provides some concluding remarks.

2. Diagnostic method of vorticity development

In an adiabatic frictionless atmosphere, development of vertical vorticity is associated with the change of static stability, baroclinicity and horizontal vorticity under the restriction of conserved potential vorticity (PV). Since the commonly used vertical vorticity equation (referred to as the "classical vertical vorticity equation"; Wu, 2001; Holton, 2004) is derived from the momentum equation, these thermodynamic effects associated with static stability, baroclinicity and horizontal vorticity are thus not involved in the forcing of vertical vorticity development. In order to describe the impacts of these thermodynamic factors on the evolution of vertical vorticity and the associated inner dynamics, Wu and Liu (1999) derived a complete form of the vertical vorticity equation (CVE) from the PV equation and developed the slantwise vorticity development theory (SVD; Wu et al., 1995; Wu and Cai, 1997), which can explain the explosive increase of vertical vorticity during the frontal rainfall process. The PV equation and the corresponding CVE (Wu and Liu, 1999) in the z-coordinate can be written as

$$\frac{dP_{\mathrm{E}}}{dt} = \alpha\nabla\theta\cdot\boldsymbol{F} + \alpha\boldsymbol{\zeta}_{\mathrm{a}}\cdot\nabla Q\,, \tag{1}$$

and

$$\begin{aligned}\frac{d}{dt}\zeta = {} & -\beta v - \zeta_{\mathrm{a}}\nabla\cdot\boldsymbol{v} - \frac{\boldsymbol{\zeta}_{\mathrm{h}}\cdot\nabla_{\mathrm{h}}\theta}{\theta_{\mathrm{z}}}\nabla\cdot\boldsymbol{v} - \frac{\zeta_{\mathrm{a}}}{\theta_{\mathrm{z}}}\frac{d}{dt}\theta_{\mathrm{z}} \\ & - \frac{\zeta_{\mathrm{h}\theta}}{\theta_{\mathrm{z}}}\frac{d}{dt}|\nabla_{\mathrm{h}}\theta| - \frac{|\nabla_{\mathrm{h}}\theta|}{\theta_{\mathrm{z}}}\frac{d}{dt}\zeta_{\mathrm{h}\theta} \\ & + \frac{1}{\theta_{\mathrm{z}}}(\nabla\theta\cdot\boldsymbol{F} + \boldsymbol{\zeta}_{\mathrm{a}}\cdot\nabla Q)(\theta_{\mathrm{z}}\neq 0)\,,\end{aligned} \tag{2}$$

respectively, where $P_{\mathrm{E}} = \alpha\boldsymbol{\zeta}_{\mathrm{a}}\cdot\nabla\theta$ is the Ertel PV; $\alpha = 1/\rho$ is the specific volume; $\boldsymbol{\zeta}_{\mathrm{a}} = (\partial w/\partial y - \partial v/\partial z, \partial u/\partial z - \partial w/\partial x, \partial v/\partial x - \partial u/\partial y + f)$ is the 3D absolute vorticity vector; $\theta = T(p_s/p)^{R/c_p}$ is the potential temperature; T is temperature; p is pressure; p_s is the reference pressure; R is the dry-air gas constant; c_p is the specific heat at constant pressure; $\nabla = (\partial/\partial x)\boldsymbol{i} + (\partial/\partial y)\boldsymbol{j} + (\partial/\partial z)\boldsymbol{k}$ is the three-dimensional gradient operator; $\boldsymbol{F}$ is the force of friction; Q is the diabatic heating, which contains latent heat release by water vapor condensation; ζ is the relative vertical vorticity; $\zeta_{\mathrm{a}} = \zeta + f$ is the absolute vertical vorticity, where f is the Coriolis parameter; $\beta = \partial f/\partial y$ is the longitudinal change of f; $V = (u, v, w)$ is the 3D velocity vector; $\boldsymbol{\zeta}_{\mathrm{h}} = (\partial w/\partial y - \partial v/\partial z, \partial u/\partial z - \partial w/\partial x, 0)$ is the horizontal vorticity vector; $\theta_{\mathrm{z}} = \partial\theta/\partial z$ is the static stability; $\nabla_{\mathrm{h}}\theta = (\partial/\partial x)\theta\boldsymbol{i} + (\partial/\partial y)\theta\boldsymbol{j}$ is the horizontal potential temperature gradient; and $\zeta_{\mathrm{h}\theta} = |\boldsymbol{\zeta}_{\mathrm{h}}|\cos(\langle\boldsymbol{\zeta}_{\mathrm{h}}, \nabla_{\mathrm{h}}\theta\rangle)$ is the projection of the horizontal vorticity vector $\boldsymbol{\zeta}_{\mathrm{h}}$ along $\nabla_{\mathrm{h}}\theta$.

In Eq. (2), the first two terms on its right-hand side are the β effect term and the divergence term, which are also contained in classical vertical vorticity equation. The third to sixth terms are seen as thermodynamic processes contributing to vertical vorticity development, which are, respectively, the time change of specific volume, static stability, baroclinicity, and horizontal vorticity. In addition, friction dissipations and diabatic heating effects are contained in the seventh and eighth terms. In the previous almost 20 years since the development of SVD theory and the CVE, numerous studies (e.g., Cui et al., 2002; Meng et al., 2004; Li et al., 2005) have shown that static stability, vertical wind shear and baroclinicity all play important roles in the rapid (even explosive) increase of vertical vorticity under the slant of isentropic surfaces, which is usually associated with severe hazardous weather. For example, Yu and Wu (2001) showed that due to the steep orientation of moist isentropic surfaces, moist baroclinicity can trigger slantwise development of vertical vortic-

ity, which may induce the rapid development of a tropical cyclone; Wang et al. (2010) investigated a heavy snowfall case caused by the northward procession of a Bay of Bengal tropical storm, with MPV and SVD theory; and Wu et al. (2013) and Zheng et al. (2013) extended SVD theory into a generalization sense under a PV-θ view, and with this diagnostic tool they showed that horizontal vorticity and baroclinicity make a positive contribution to Tibetan Plateau low vortex development.

In this paper, deformation strain is introduced into a diagnosis of vertical vorticity by the fifth term of Eq. (2); that is, the individual difference term of baroclinicity. This is based on the fact that deformation has been shown as the most important mechanism driving frontogenesis or the increase in baroclinicity, either by idealized numerical studies or by the frontogenesis function (e.g., Hoskins and Bretherton, 1972; Keyser and Anthes, 1982; Davies and Müller, 1988; Keyser et al., 1988). By coupling the CVE and frontogenesis function, a mathematical relation between deformation and vorticity can be built.

The derivation begins with a generalization of the CVE into a moist baroclinic atmosphere due to the often close relation between strong vorticity and heavy rainfall; that is, the latent heat release caused by the water vapor phase change is considered. In the CVE, expressed by Eq. (2), latent heat is attributed to Q, which it is not possible to calculate accurately with conventional observations or reanalysis data. For the flexible use of general reanalysis data, the moist PV (MPV) in the p-coordinate is used as follows:

$$P_{\rm m} = -g(\nabla \times \boldsymbol{V}_{\rm h}) \cdot \nabla \theta_{\rm e} = -g \left[\boldsymbol{\zeta}_{\rm h} \cdot \nabla \theta_{\rm e} + (\zeta + f) \frac{\partial \theta_{\rm e}}{\partial p} \right] , \tag{3}$$

where $\boldsymbol{\zeta}_{\rm h} = (-\partial v/\partial p, \partial u/\partial p)$ is the horizontal vorticity vector, $\theta_{\rm e} = \theta \exp(Lq/c_p T)$ is the equivalent potential temperature, L is the latent heat, and q is the specific humidity. Note that the horizontal vorticity resulting from the vertical velocity is ignored in Eq. (3), mainly due to its small value compared with the horizontal vorticity resulting from vertical wind shear. However, this treatment is not applicable to a convective atmosphere where the magnitude of vertical velocity is comparable to the horizontal velocities. By the vorticity equation, the continuity equation and thermodynamic equation in the p-coordinate, the MPV equation can be derived (Wu et al., 1995) as

$$\frac{d}{dt} P_{\rm m} = -g \nabla \times \boldsymbol{F} \cdot \nabla \theta_{\rm e} - g \boldsymbol{\zeta}_{\rm a} \cdot \nabla Q_{\rm m} , \tag{4}$$

where g is gravitational acceleration, $\nabla_{\rm p} = (\partial/\partial x)\boldsymbol{i} + (\partial/\partial y)\boldsymbol{j}$ is the gradient operator in the p-coordinate, and $Q_{\rm m}$ is the diabatic heating rate apart from the latent heat. With Eq. (4), the complete form of the vertical vorticity equation in the p-coordinate can be derived:

$$\begin{aligned} \frac{d}{dt}\zeta = {} & -\beta v - \frac{\zeta_{\rm a}}{\theta_{\rm ep}} \frac{d}{dt}\theta_{\rm ep} - \frac{\zeta_{{\rm h}\theta_{\rm e}}}{\theta_{\rm ep}} \frac{d}{dt}|\nabla_{\rm p}\theta_{\rm e}| - \frac{|\nabla_{\rm p}\theta_{\rm e}|}{\theta_{\rm ep}} \frac{d}{dt}\zeta_{{\rm h}\theta_{\rm e}} \\ & + \frac{1}{\theta_{\rm ep}} \nabla \times \boldsymbol{F} \cdot \nabla \theta_{\rm e} + \frac{1}{\theta_{\rm ep}} \boldsymbol{\zeta}_{\rm a} \cdot \nabla Q_{\rm m} , \end{aligned} \tag{5}$$

where $\theta_{\rm ep} = \partial \theta_{\rm e}/\partial p$ is convective stability, and $\zeta_{{\rm h}\theta_{\rm e}}$ is the projection of the horizontal vorticity vector $\boldsymbol{\zeta}_{\rm h} = (-\partial v/\partial p, \partial u/\partial p)$ along $\nabla_{\rm p}\theta_{\rm e}$. In Eq. (5), the first term on the right-hand side is the β effect term or the change of planetary vorticity, the second term is the temporal change term of the convective stability, the third term is the temporal change term of moist baroclinicity, the fourth term is the temporal change term of vertical wind shear, the fifth term is the friction term, and the sixth term is the effect of adiabatic processes.

In a further step, the moist frontogenesis function is introduced, which is often used to diagnose the frontogenesis instead of the original frontogenesis function when there is precipitation (Bluestein, 1993):

$$F = \frac{d}{dt}|\nabla_{\rm p}\theta_{\rm e}| = F_{\rm G1} + F_{\rm G2} + F_{\rm G3} + F_{\rm G4} ; \tag{6}$$

$$F_{\rm G1} = -\frac{D}{2}|\nabla_{\rm p}\theta_{\rm e}| ; \tag{7}$$

$$\begin{aligned} F_{\rm G2} &= -\frac{1}{2|\nabla_{\rm p}\theta_{\rm e}|} \left[E_{\rm st} \left(\frac{\partial \theta_{\rm e}}{\partial x} \right)^2 + 2E_{\rm sh} \frac{\partial \theta_{\rm e}}{\partial x} \frac{\partial \theta_{\rm e}}{\partial y} - E_{\rm st} \left(\frac{\partial \theta_{\rm e}}{\partial y} \right)^2 \right] \\ &= \frac{|\nabla_{\rm p}\theta_{\rm e}|}{2} |E| \cos 2\gamma ; \end{aligned} \tag{8}$$

$$F_{\rm G3} = -\frac{1}{|\nabla_{\rm p}\theta_{\rm e}|} \left(\frac{\partial \omega}{\partial x} \frac{\partial \theta_{\rm e}}{\partial x} + \frac{\partial \omega}{\partial y} \frac{\partial \theta_{\rm e}}{\partial y} \right) \frac{\partial \theta_{\rm e}}{\partial p} ; \tag{9}$$

$$F_{\rm G4} = \frac{1}{|\nabla_{\rm p}\theta_{\rm e}|} \left[\frac{\partial \theta_{\rm e}}{\partial x} \frac{\partial Q_{\rm m}}{\partial x} + \frac{\partial \theta_{\rm e}}{\partial y} \frac{\partial Q_{\rm m}}{\partial y} \right] . \tag{10}$$

Here, $F_{\rm G1}$ is the divergence term, $F_{\rm G2}$ is the deformation term, $F_{\rm G3}$ is the tilting term, and $F_{\rm G4}$ is the diabatic term. D is horizontal divergence, $E_{\rm st}$ is horizontal stretching deformation, $E_{\rm sh}$ is horizontal shearing deformation, and γ is the angle between the equivalent potential temperature contours and the dilatation axis, which controls the effect of deformation on front development. When $\gamma < 45^\circ$, there is deformational moist frontogenesis, and when $\gamma > 45^\circ$ there is deformational moist frontolysis.

Equation (6) is directly substituted into the moist baroclinicity term in the CVE [Eq. (5)], and the CVE in p-coordinates can thus be written as

$$\frac{\partial}{\partial t}\zeta = F_{\zeta 1} + F_{\zeta 2} + F_{\zeta 3} + F_{\zeta 4} + F_{\zeta 5} , \tag{11}$$

where the β effect, frictions and diabatic heating have been ignored, and:

(1) $F_{\zeta 1} = -\boldsymbol{V}_{\rm h} \cdot \nabla_{\rm p}\zeta$ is horizontal advections of vertical vorticity;

(2) $F_{\zeta 2} = -\omega(\partial\zeta/\partial p)$ is vertical advection of vertical vorticity;

(3) $F_{\zeta 3} = -(\zeta_{\rm a}/\theta_{\rm ep})(d\theta_{\rm ep}/dt)$ is the time variation term of convective stability;

(4) $F_{\zeta 4} = -(\zeta_{{\rm h}\theta_{\rm e}}/\theta_{\rm ep})(d|\nabla_{\rm p}\theta_{\rm e}|/dt) = -(\zeta_{{\rm h}\theta_{\rm e}}/\theta_{\rm ep})(F_{\rm G1} + F_{\rm G2} + F_{\rm G3}) = F_{\zeta 41} + F_{\zeta 42} + F_{\zeta 43}$ is the time variation term of moist baroclinicity, in which

$$F_{\zeta 41} = -\frac{\zeta_{{\rm h}\theta_{\rm e}}}{\theta_{\rm ep}} F_{\rm G1} = \frac{\zeta_{\rm h} \cdot \nabla_{\rm p}\theta_{\rm e}}{2\theta_{\rm ep}} D , \tag{12}$$

is the vertical vorticity development caused by divergence-induced moist baroclinicity variation,

$$F_{\zeta 42} = -\frac{\zeta_{h\theta_e}}{\theta_{ep}} F_{G2} = -\frac{\zeta_h \cdot \nabla_p \theta_e}{2\theta_{ep}} |E| \cos 2\gamma \,, \qquad (13)$$

is the impact of deformation-induced moist baroclinicity variation on vertical vorticity development, and

$$F_{\zeta 43} = -\frac{\zeta_{h\theta_e}}{\theta_{ep}} F_{G3} = \frac{\zeta_{h\theta_e}}{\theta_{ep}} \frac{1}{|\nabla_p \theta_e|} \left(\frac{\partial \omega}{\partial x} \frac{\partial \theta_e}{\partial x} + \frac{\partial \omega}{\partial y} \frac{\partial \theta_e}{\partial y} \right) \frac{\partial \theta_e}{\partial p} \,, \qquad (14)$$

is the vertical vorticity development caused by the horizontal inhomogeneous distribution of vertical motions;

(5) $F_{\zeta 5} = -(|\nabla_p \theta_e| / \theta_{ep})(d/dt)\zeta_{h\theta_e}$ is the time variation term of vertical wind shear (or horizontal vorticity).

In all of the above forcing terms in the CVE, it can be seen that deformation is directly contained in the baroclinicity variation–related term $F_{\zeta 42}$, which then affects development of vertical vorticity. From $F_{\zeta 42}$, it is shown that whether deformation can induce vorticity development not only depends on deformation itself, but also the atmospheric thermodynamic background; that is, the convective stability, vertical wind shear and baroclinicity. These are explicitly diagnosed in the following case study.

3. Case study

With the above theoretical theorems [Eqs. (13) and (11)], the impact of deformation on vorticity development is studied in a heavy-rainfall event that occurred in a strong moist baroclinic environment. The data for the analysis are from the NCEP (National Centers for Environmental Prediction) global reanalysis dataset, with a horizontal resolution of $0.5^\circ \times 0.5^\circ$. Figure 1 shows the precipitation distribution of the studied case, which occurred during 20–22 July 2012. As shown in Fig. 1, the precipitation has an evident belt structure, oriented in a northeast–southwest direction. On 20 July (Fig. 1a), the rainbelt is mainly located northwest of China, with three heavy-precipitation centers in Inner Mongolia (labelled A), the joint areas ofShaanxi, Ningxia and Gansu provinces (B), and north of the Sichuan Basin (C). On 21 July (Fig. 1b), the rainbelt displaces southeastward and elongates, also with three heavy-precipitation centers. In Fig. 1b, center A, which has the heaviest precipitation, covers Beijing, Tianjin and part of Hebei. On this day, the averaged daily precipitation amount in Beijing reaches up to 170 mm, and the total precipitation amount reaches up to 460 mm in Hebei town of Fangshan district, which induced great economic losses and casualties. On 22 July, with the eastward movement of the rainbelt, precipitation decreases and the belt structure mainly persists in East and Northeast China.

Figure 2 shows the distributions of some basic variables in typical levels at 1200 UTC 21 July 2012, illustrating the weather configuration of this case. Corresponding to the orientation and location of the 6-h accumulated precipitation belt at 1200 UTC, there is a northeast–southwest oriented jet stream (shaded areas of Fig. 2a; wind speed >30 m s^{-1}) in

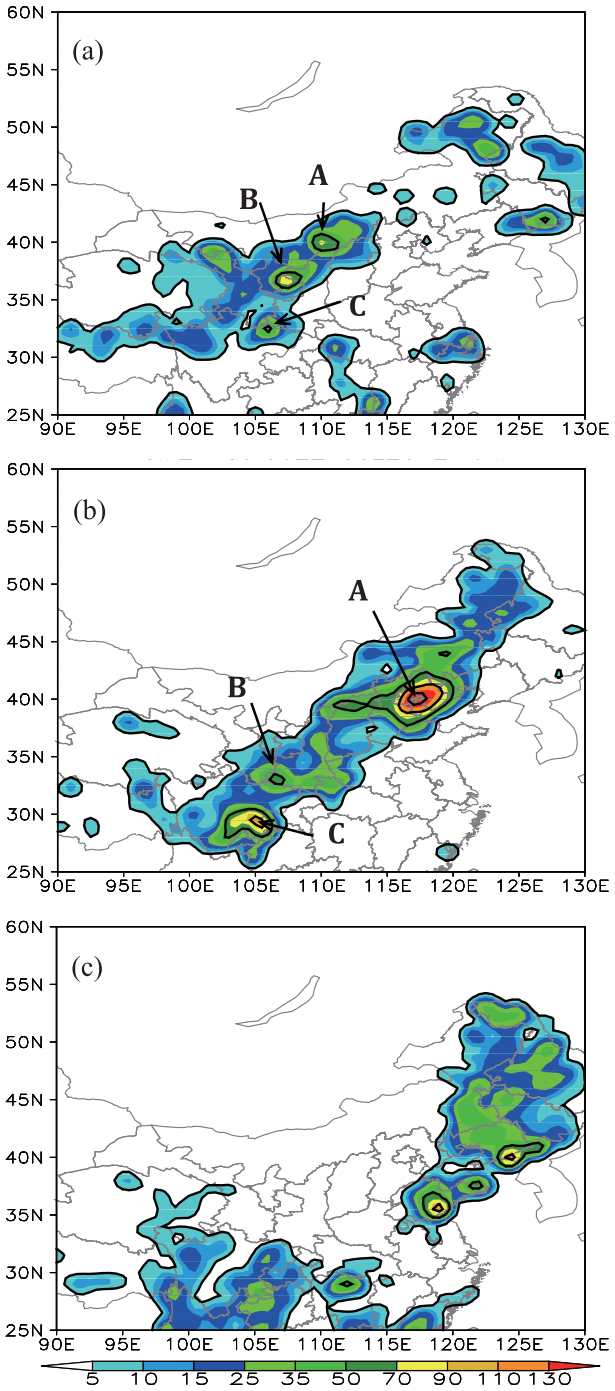

Fig. 1. The 24-h observational accumulated precipitation during 20–22 July 2012 (units: mm).

the 200 hPa upper level and a moist strong baroclinic zone (cold front; black lines in Fig. 2a) at 700 hPa in the lower troposphere. The heavy rainfall is closely related to this cold front. The front leads the cold air mass southward, and encounters warm-moist air flow from low latitudes, which induces strong precipitation along the cold front. In the mid-level (Fig. 2b), the precipitation area is characterized by deformational flow, with cyclonic wind shear (low trough at the bottom of the cyclone, centered over Lake Baikal) on the north side of the rainbelt, which causes cold-air intrusion in

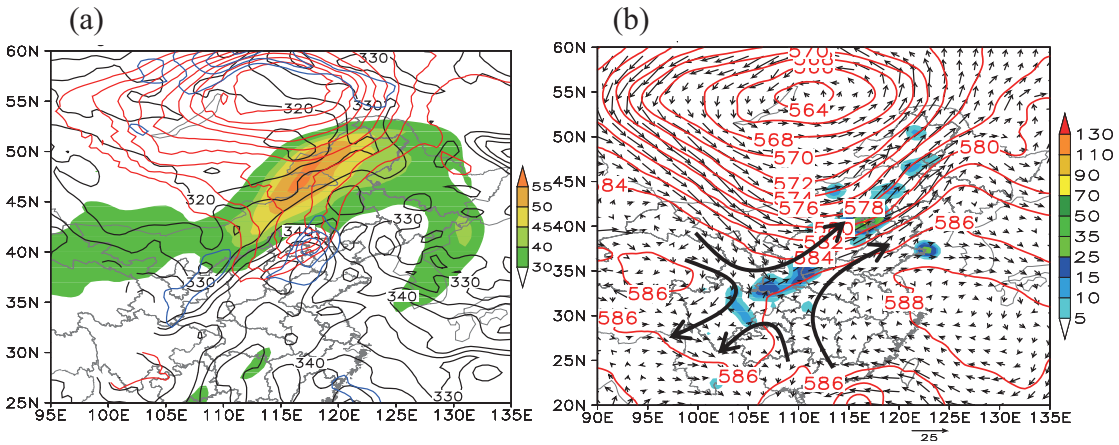

Fig. 2. (a) Horizontal wind speed at 200 hPa (colored areas; units: m s^{-1}), equivalent potential temperature (black solid lines; units: K), geopotential height (red solid lines; units: 10 gpm) and horizontal wind speed (>12 m s^{-1}; blue solid lines; units: m s^{-1}) at 700 hPa. (b) Horizontal wind field (black arrows) and geopotential height (red solid lines) at 500 hPa, and 6-h observational accumulated precipitation (colored areas; units: mm) at 1200 UTC 21 July 2012.

the mid-level and tends to strengthen the rainfall. In addition, the 500 hPa southwesterly prevailing over the areas of Hebei, Beijing and Tianjin also leads meso-γ scale convective cells moving northeasterly. This so-called steering flow has an impact on the 'echo-training' mechanism of the 'Beijing 721 heavy rainfall' event. As apparent in Fig. 2, another evident feature of the weather pattern is a meso-β scale low vortex (about 500 km in length) in the most severe precipitation area (about 41°N, 116.5°E). The low vortex is collocated with the low-level jet at 700 hPa (wind speed >12 m s^{-1}; blue lines in Fig. 2a). In Fig. 2a, the low-level geopotential height (red lines) shows the mesoscale low vortex to be connected to the large vortex in the vicinity of Lake Baikal, overlaying the strong baroclinic zone or cold front. Strong coherent rotation caused by the low vortex plays a significant role in the persistence of the precipitating system, which provides a favorable environment for the concentration of energy and transport. In the whole process of the studied rainfall case, the strongest precipitation center is collocated with, and moves with, the vortex. As shown in Fig. 3, which gives the movement of the low vortex with the three-day averaged geopotential height at 700 hPa as a background, the low vortex develops and moves in a typical saddle-shaped field with two highs and two lows alternatively distributed. In the high latitudes, a high ridge is located west of Lake Baikal, while a low vortex is located west of the lake. In the low latitudes is a low vortex over the Bay of Bengal, south of the Tibetan Plateau (approximately 80°–90°E), and a subtropical high over the east of China over the ocean. A large-scale deformation field then forms over the north and northwest of China, plus the blocking effect of the Tibetan Plateau. As the low vortex initializes on the northeast edge of the Tibetan Plateau, it moves northeastward along the dilation axis of the large-scale deformation field, which influences the provinces of Shaanxi, Shanxi, Hebei, Liaoning and Jilin, successively. The saddle-shaped weather pattern is a typical deformation field in the atmosphere. Evolution of the low vortex in the saddle-shaped weather pattern,

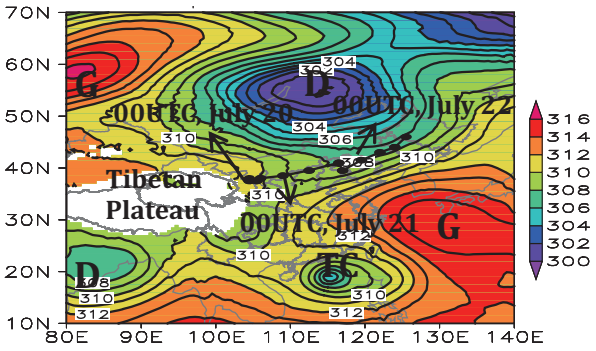

Fig. 3. Three-day time-averaged geopotential height at 700 hPa during 20–22 July 2012 (units: 10 gpm). The black dot is the location of the low vortex center at different times, and the lines between indicate the direction of movement of the low vortex.

or in the large-scale deformation field, shows that deformation may have played an important role in the vortex's development, which has been noted in several other studies. For example, with an idealized numerical experiment, Jiang (2011) showed that the deformational field has an important impact on the formation of a meso-β scale vortex. Through statistical analysis of the boundary deformation fields during the Mei-yu period, Deng (1986) stated that deformation can be applied to indicate the movement and development of low vortex systems. However, to explicitly identify the relation of the deformation field and vortex development, further quantitative diagnosis would be necessary. In the following part of the study, the impact of deformation on the evolution of the low vortex in the strong baroclinic frontal zone is diagnosed.

3.1. *Vortex evolution*

According to the interactions of the low vortex and the cold front, the lifecycle of the vortex is decomposed into four stages: the initial stage, development stage, maturation stage, and dissipating stage (Fig. 4 and Table 1). In the initial stage

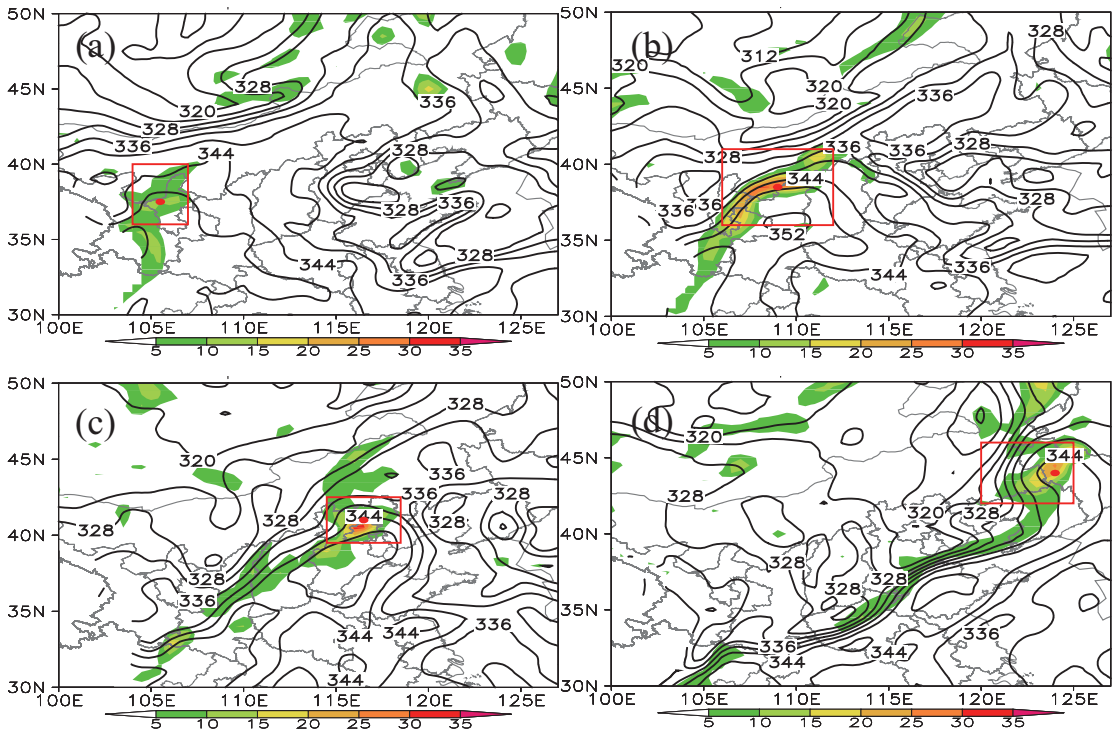

Fig. 4. Vortex evolution denoted by vertical vorticity (colored areas; units: 10^{-5} s^{-1}): (a) initial stage at 1200 UTC 20 July; (b) development stage at 0000 UTC 21 July; (c) mature stage at 1200 UTC 21 July; (d) dissipating stage at 0600 UTC 22 July 2012. The black solid lines are equivalent potential temperature.

Table 1. Development stages of the low vortex.

Time	Vortex center	Stage	Key area	Influence level
1200 UTC 20 July	(37.5°N, 105.5°E)	Initiation	(36°–40°N, 104°–107°E)	~650 hPa
1800 UTC 20 July	(38.0°N, 106.0°E)	Initiation	(36.5°–40.5°N, 104.5°–108.5°E)	800–550 hPa
0000 UTC 21 July	(38.5°N, 109.0°E)	Development	(36°–41°N, 106°–112°E)	800–600 hPa
0600 UTC 21 July	(39.5°N, 112.5°E)	Maturation	(37.5°–41.5°N, 109.5°–115°E)	800–600 hPa
1200 UTC 21 July	(41.0°N, 116.5°E)	Maturation	(39.5°–42.5°N, 114.5°–118.5°E)	800–600 hPa
1800 UTC 21 July	(39.5°N, 117.0°E)	Maturation	(36°–40°N, 104°–107°E)	925–700 hPa
0000 UTC 22 July	(41.5°N, 119.5°E)	Maturation	(36°–40°N, 104°–107°E)	925–600 hPa
0600 UTC 22 July	(43.0°N, 122.0°E)	Dissipation	(36°–40°N, 104°–107°E)	925–600 hPa
1200 UTC 22 July	(44.0°N, 124.0°E)	Dissipation	(36°–40°N, 104°–107°E)	950–700 hPa
1800 UTC 22 July	(46.0°N, 125.5°E)	Dissipation	(36°–40°N, 104°–107°E)	950–750 hPa

at 1200 UTC 20 July (Fig. 4a), the strong baroclinic frontal zone is on the north border of China (about 42°N). The low vortex, denoted by the large positive vertical vorticity area, forms in the warm sector of the front, influenced by the prefrontal warm moist flow. After initiation, with the southward intrusion of the cold front, the vortex is gradually superposed over the cold front and develops substantially (Fig. 4b). Then, the vortex (large positive vorticity anomalies) moves northeastward within the front and enters the Beijing area at 1200 UTC 21 July (Fig. 4c), when severe heavy precipitation occurs over Beijing. Meanwhile, the vortex reaches its maturation stage. Subsequently, with longitudinal enlargement of the cold front, the vortex gradually separates with the front and dissipates (Fig. 4d), showing a tendency to merge with the high-latitude cyclone (figure omitted).

3.2. *Deformation-induced vorticity development diagnosis*

The deformation related term $F_{\zeta 42}$ [Eq. (13)] is calculated over every stage of the vortex to diagnose the impact of deformation on the vortex's development. Figure 5 shows the vertical distributions of $F_{\zeta 42}$ along the vortex center. As shown in Fig. 5a, in the initial stage, the positive vorticity area over the formation location (37.5°N, 105.5°E) of the vortex stretches from the surface (approximately 800 hPa over the terrain) up to 600 hPa, with the center close to the surface (about 16×10^{-5} s^{-1}). The deformation-related term $F_{\zeta 42}$ mainly presents negative values over the positive vorticity area, which implies that deformation suppresses the in-

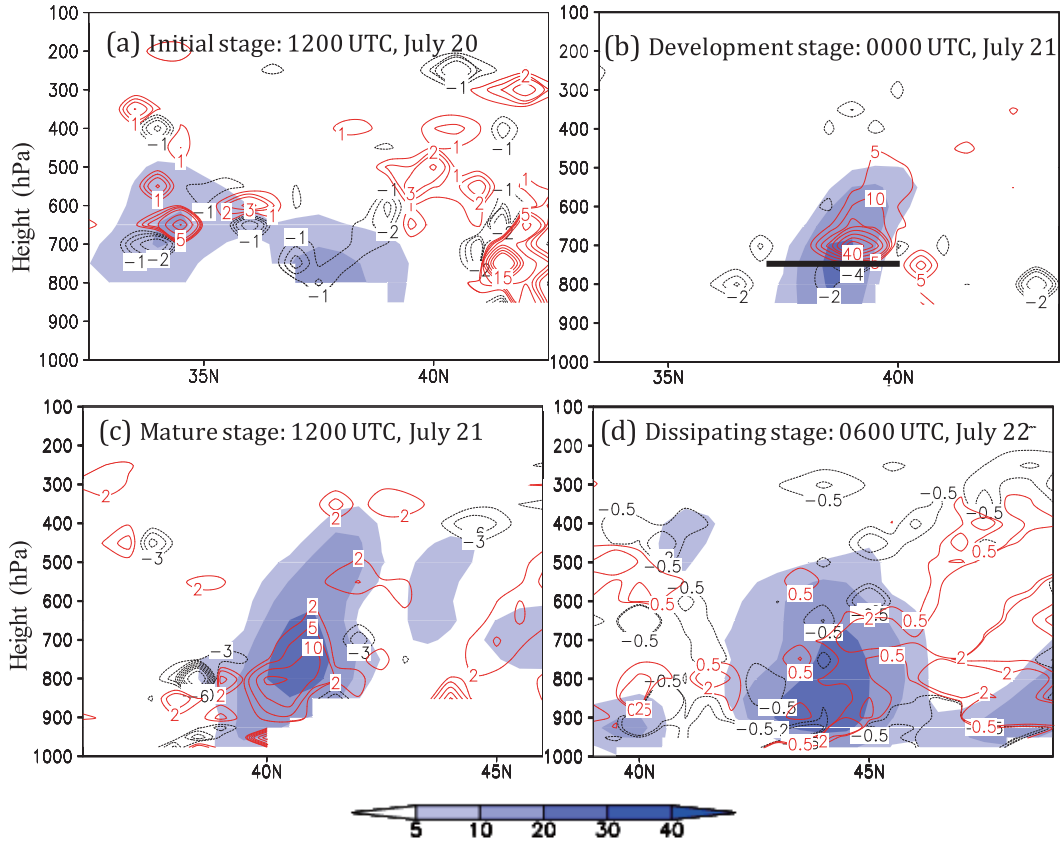

Fig. 5. Vertical distribution of the deformation-related vorticity development term $F_{\zeta 42}$ (units: 10^{-9} s^{-2}) along the longitude passing through the vortex center (Table 1): (a) initial stage at 1200 UTC 20 July; (b) development stage at 0000 UTC 21 July; (c) mature stage at 1200 UTC 21 July; (d) dissipating stage at 0600 UTC22 July 2012. The black solid lines are negative values; red lines are positive values. The colored areas are vertical vorticity. (units: 10^{-5}s^{-1})

crease of positive vorticity and thus acts against the vortex's initiation. As shown in Fig. 5b, in the development stage of the vortex at 0000 UTC 21 July, positive vertical vorticity presents a significant increase and forms a coherent vorticity column, stretching from the surface up to 500 hPa, with the center at about 750 hPa (30×10^{-5} s^{-1}). In this stage, with the southward intrusion of the cold front into the vortex, the impact of deformation on vertical vorticity development changes evidently. In Fig. 5b, over the vorticity column, the deformation-related term $F_{\zeta 42}$ shows positive values above 750 hPa and negative values below 750 hPa. The positive center (60×10^{-9} s^{-2}) is approximately at the 700 hPa level, with the intensity much stronger than the negative center. This means that, in the development stage, deformation changes to increase the vertical vorticity and promote the vortex's development, with the most evident effect at 700 hPa. After the explosive genesis in the development stage, the vortex evolves into a slow-developing maturation stage, as shown in Fig. 5c. In this stage, the vortex enters North China and influences the Heibei–Beijing–Tianjin area, inducing extreme precipitation. At 1200 UTC 21 July, the vortex center is at about 41°N and the associated vorticity column shows a downward sliding to the plain, with the length and height much larger than in the previous two stages. Over the vorticity column, the deformation-related term $F_{\zeta 42}$ shows all positive values, stretching from the boundary (900 hPa) up to 600 hPa. This means, in the maturation stage, deformation also plays a role in promoting the vortex's development, albeit with a much weaker intensity. After the maturation stage, the vortex gradually moves out of North China and enters the Northeast Plain. Along the vortex center at about 43°N, the positive vorticity column persists, with the deformation-related term $F_{\zeta 42}$ scattered in its distribution, but shows an increasing-vorticity pattern north of 44°N (black solid curve in Fig. 5d).

The above analysis highlights the fact that, in the real atmosphere, deformation can indeed induce the development of vertical vorticity, although the specific effects may depend on the temporal dynamic and thermodynamic configurations. The relative importance of the deformation-related term compared with other terms in the CVE is estimated by calculating the budget of every term in the CVE over the vortex center area in its each stage. Note that the levels that are chosen to give the calculation are a little different in different stages due to the vertical variation of the deformation-related term with time (Fig. 5). In Fig. 6, it is shown that the primary

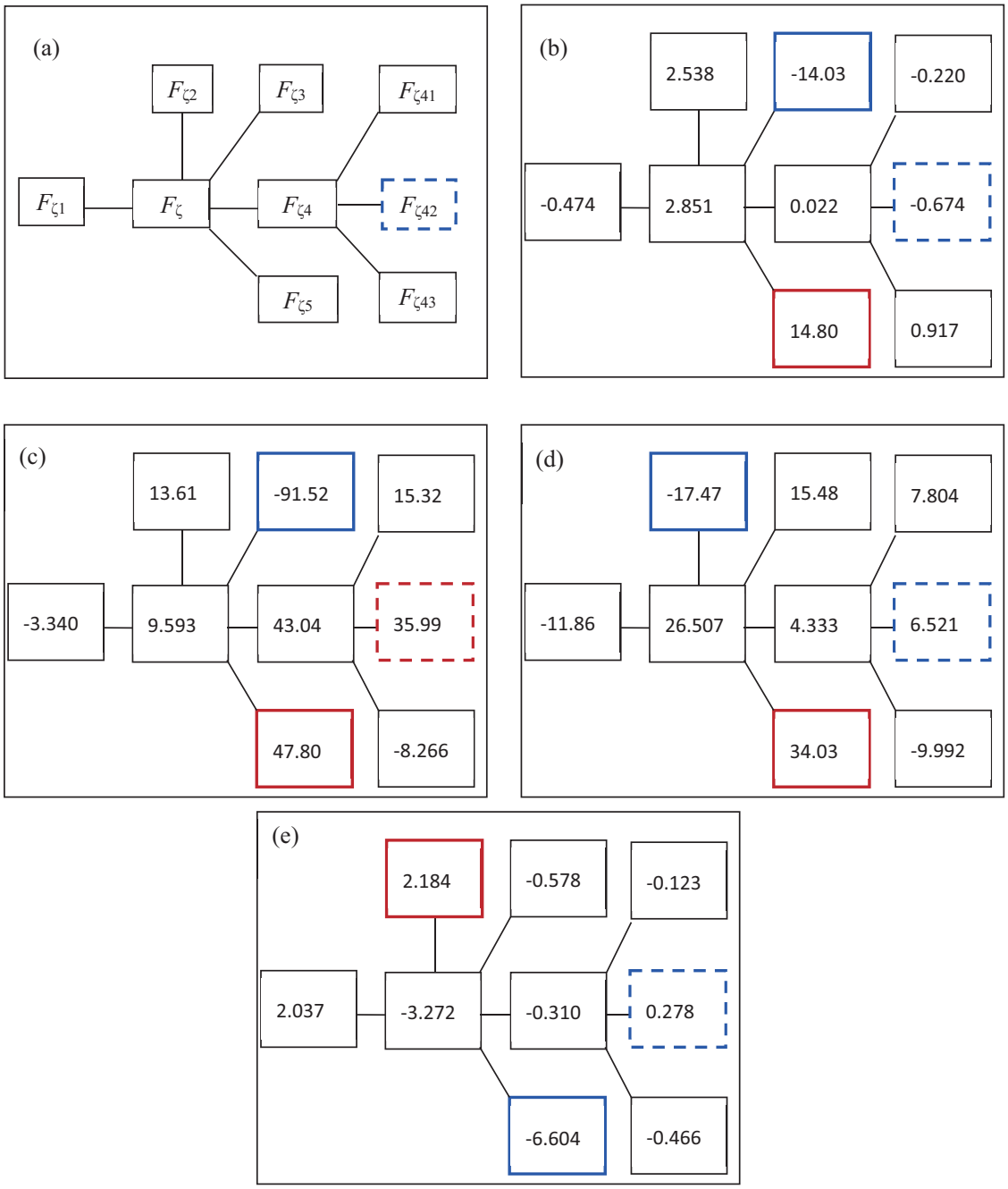

Fig. 6. Vertical vorticity budget in the vortex center area obtained by Eq. (11) during 20–22 July 2012: (a) sketch map of every term; (b) averaged budget over (37.0°–38.0°N, 105.0°–106.0°E) at 700 hPa at 1200 UTC 20 July; (c) averaged budget over (38.0°–39.0°N, 108.5°–109.5°E) at 700 hPa at 0000 UTC 21 July; (d) averaged budget over (40.5°–41.5°N, 116.0°–117.0°E) at 800 hPa at 1200 UTC 21 July; (e) averaged budget over (43.5°–44.5°N, 123.5°–124.5°E) at 850 hPa at 1200 UTC 22 July. The red (blue) box is the main term increasing (decreasing) positive vertical vorticity. The blue dotted box is the deformation-related term.

factor that contributes to the vortex's development presents a significant difference. In the initial stage (Fig. 6b), the total forcing [sum of the terms on the right-hand side of Eq. (11)] is positive, which corresponds to the increase in vertical vorticity and formation of the vortex. The vertical wind shear term $F_{\zeta 5}$ makes the largest contribution to the vortex's formation, while the convective stability–variation term $F_{\zeta 3}$ suppresses the vortex's formation. The moist baroclinicity–variation term makes almost no contribution to the vortex's formation, although it has positive values and tends to increase the vertical vorticity. The deformation-related term $F_{\zeta 42}$ displays suppression of the vortex's development in this stage, but its magnitude is quite small. In the development stage (Fig. 6c), the vertical wind shear term $F_{\zeta 5}$ and

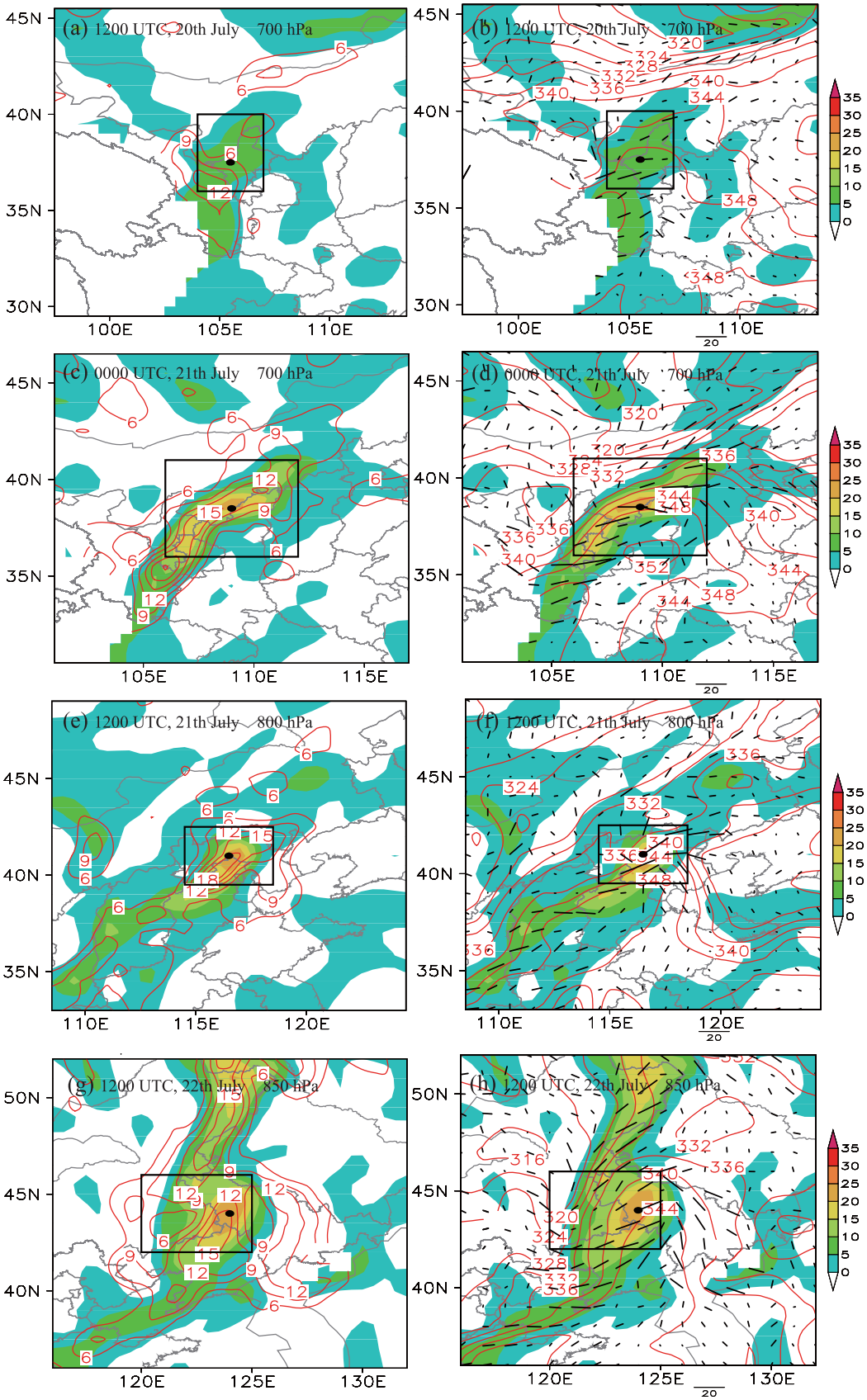

Fig. 7. Total deformation (left column; red lines; units: 10^{-5} s^{-1}) and deformation tick marks (right column; black short line; units: 10^{-5} s^{-1}). The shaded areas are vertical vorticity; the red lines in the right column are equivalent potential temperature (units: 1 K); the black box is the critical area of the vortex; and the black dots indicate the vortex center.

the convective stability–variation term $F_{\zeta 3}$ are still the two leading terms that influence the vortex's development, but with the suppression effect by $F_{\zeta 3}$ becoming almost twofold greater than the promotion effect by $F_{\zeta 5}$. However, the total forcing is still positive and the low vortex develops. This is mostly due to the increased contribution from the moist baroclinicity–variation term, which is mainly caused by the increase of the deformation-related term (Figs. 6b–c). In the maturation stage, positive total forcing maintains in the vortex center, to keep the vertical vorticity increasing. The vertical wind shear term $F_{\zeta 5}$ is still the main factor driving the vortex's development, while the vertical advection term $F_{\zeta 2}$ becomes the main suppression term instead of $F_{\zeta 3}$. At this time, the deformation-related term still promotes the vortex's development, but with a smaller contribution compared to the last stage. In the dissipating stage (Fig. 6e), the total forcing of vertical vorticity in the vortex center becomes negative. On the contrary to the maturation stage, the vertical wind shear term turns into a negative factor for vertical vorticity increasing, while the vertical advection term begins to maintain the vortex; that is, resisting the dissipation of the vortex. The deformation-related term also shows a promotion of increased vertical vorticity.

From the above analysis, the impact of deformation on vortex evolution and its magnitude is quite different in the various vortex stages. Both the vertical distributions of the deformation-related term and the vorticity budget show that, during the whole lifecycle of the low vortex, deformation has the most important effect on increasing vertical vorticity during the vortex development stage; that is, when the cold front intrudes southward into the vortex. In order to explain the specific dynamic and thermodynamic structures that are favorable to the deformation in promoting the vortex's development, the deformation-related term is the focus of discussion in the next subsection.

3.3. *The deformation-related term in the CVE*

The deformation related term [Eq. (13)] is rewritten as follows for further discussion:

$$F_{\zeta 42} = \frac{P_{\mathrm{m2}}|E|\cos 2\gamma}{2\theta_{\mathrm{ep}}}, \tag{15}$$

$$P_{\mathrm{m2}} = -\boldsymbol{\zeta}_{\mathrm{h}} \cdot \nabla_{\mathrm{p}}\theta_{\mathrm{e}} = \frac{\partial v}{\partial p}\frac{\partial \theta_{\mathrm{e}}}{\partial x} - \frac{\partial u}{\partial p}\frac{\partial \theta_{\mathrm{e}}}{\partial y}, \tag{16}$$

where the baroclinic MPV (P_{m2}; Wang et al., 1996) is applied to substitute the coupling of the vertical wind shear and the

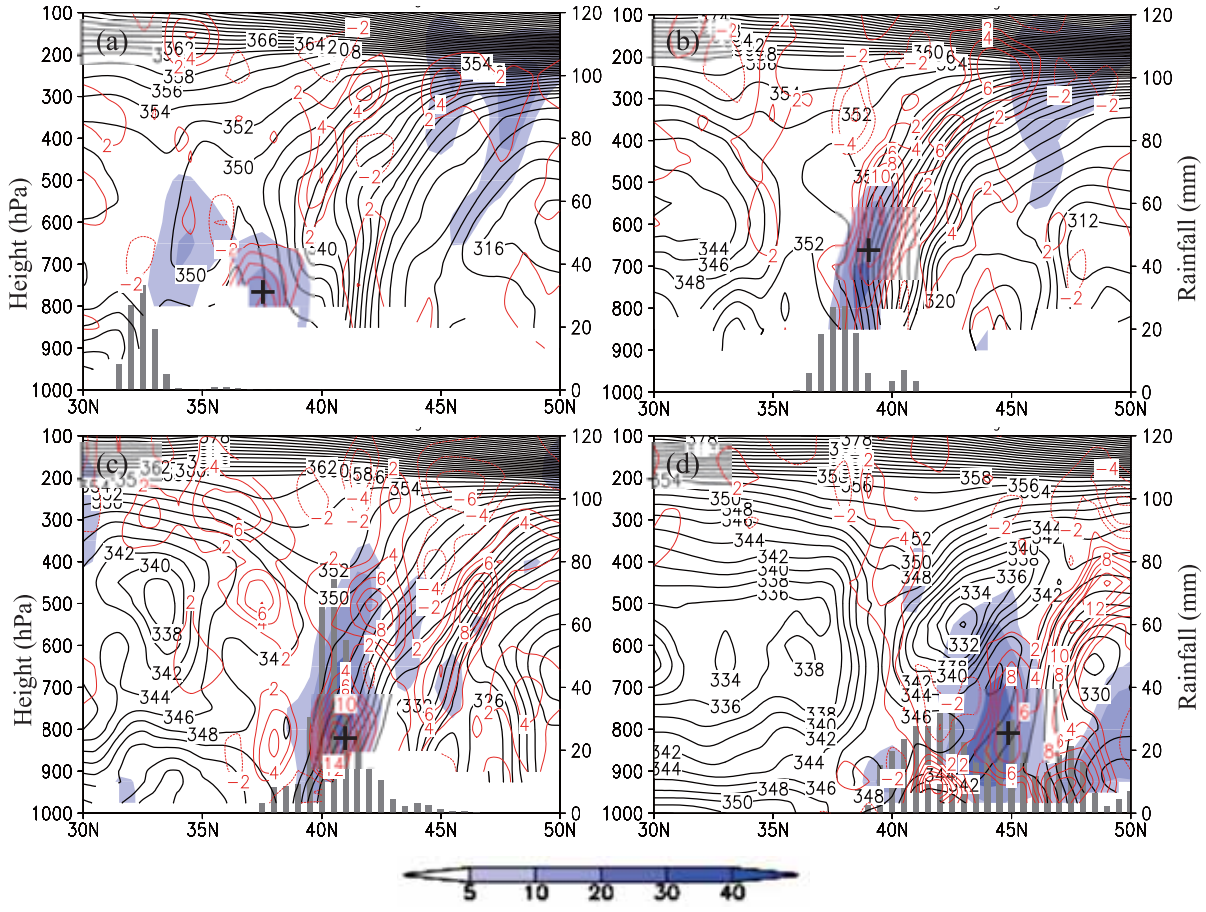

Fig. 8. Vertical distribution of $|E|\cos 2\gamma$ (red lines; units: 10^{-5} s^{-1}) along the vortex center: (a) 105.5°E at 1200 UTC 20 July; (b) 109°E at 0000 UTC 21 July; (c) 116.5°E at 1200 UTC 21 July; and (d) 124°E at 1200 UTC 22 July. The black solid lines are θ_{e} (units: K) contours, and the shaded areas are vertical vorticity (units: 10^{-5} s^{-1}). The grey bars are 6-h accumulated precipitation.

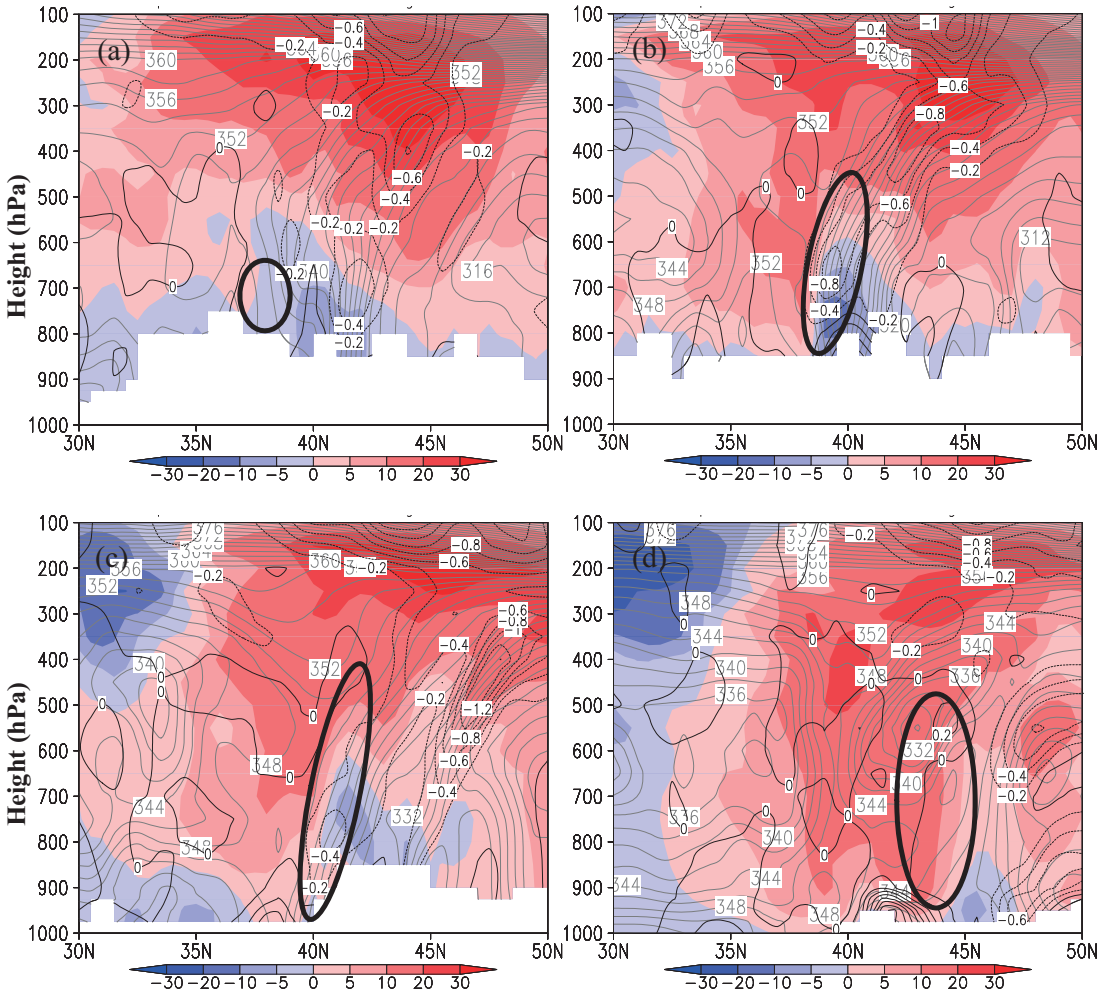

Fig. 9. Vertical distribution of P_{m2} (black lines; units: 10^{-1} PVU) along the vortex center: (a) 105.5°E at 1200 UTC 20 July; (b) 109°E at 0000 UTC 21 July; (c) 116.5°E at 1200 UTC 21 July; and (d) 124°E at 1200 UTC 22 July. The gray solid lines are θ_e (units: K) contours, and the shaded areas are zonal wind (units: m s^{-1}). The ellipses are the locations of the vorticity columns.

moist baroclinicity. Thus, from Eq. (15), the factors that influence the effect of deformation on vorticity include convective stability θ_{ep}, the baroclinic MPV (P_{m2}) and the deformation $|E|\cos 2\gamma$ (γ is the angle of the dilation axis of the deformation field and the θ_e contours). These factors are together analyzed to determine their effect on the vortex's development. Figure 7 gives the horizontal distribution of the total deformation $|E|$ and the deformation tick marks, which represent the magnitude and direction of the dilation axis of the deformation field. According to Figs. 7a, c, e and g, during the whole lifecycle of the vortex, strong deformation areas are always superposed over the vorticity belts. The magnitude of the total deformation in the vortex center in the different stages are $\sim 6\times10^{-5}$ s^{-1}, $\sim 15\times10^{-5}$ s^{-1}, $\sim 18\times10^{-5}$ s^{-1} and $\sim 15\times10^{-5}$ s^{-1}, which implies that, after initiation, the total deformation of the central vortex area maintains a steady state. Since the total deformation is always positive, the sign of $|E|\cos 2\gamma$ thus depends on the angle between the deformation dilation axis and the θ_e contours, which can be seen from Figs. 7b, d, f and h. Because of the southwest warm, moist flow into the inner land, the vortex is basically under the control of a warm ridge, seen from the convex θ_e contours. In the warm ridge, the deformation tick marks are basically aligned with the θ_e contours. West of the ridge, the tick marks are southwest–northeast or west–east oriented, while east of the ridge the tick marks become northwest–southeast oriented with the curve of the θ_e contours. This means, in the large vorticity areas, deformation always presents frontogenesis; that is, $|E|\cos 2\gamma > 0$, which can also be seen from Fig. 8. In the vertical cross sections along the vortex center (Fig. 8), the deformation term $|E|\cos 2\gamma > 0$ is always positive during the whole lifecycle of the vortex, either when the front intrudes into the vortex or not. Figure 9 gives the vertical distributions of the baroclinic MPV (P_{m2}) along the vortex center. From Fig. 9, P_{m2} mainly shows negative values over the vortex during its whole lifecycle. This is mostly due to the superposition of the high-level westerly over the low-level easterly ($\partial u/\partial p < 0$) and the moist baroclinicity

caused by the encountering of high-latitude cold air mass and low-latitude warm moist flow ($\partial\theta_e/\partial y < 0$). The configuration of the deformation term and the baroclinic MPV make the numerator of Eq. (15) mainly present negative values over the vortex area, which implies that whether or not the deformation increases the vertical vorticity depends on convective stability. In the initial stage, the vortex lies in the prefrontal unstable stratification (Fig. 10a; $\theta_{ep} > 0$); thus, the deformation-related term suppresses the vortex initiation (Fig. 5a). In the development stage, the front gradually intrudes into the vortex. The atmosphere is stable above 750 hPa and unstable below 750 hPa, which means a neutral stratification exists between these two air layers. This results in the deformation-related term showing a large positive-value center in the near-neutral layer, deriving a vertical vorticity increase above the neutral layer and decreasing it below the layer (Fig. 5b). This neutral stratification is also the main reason that deformation plays a most evident role in the vorticity increase during the vortex development stage, compared with other stages. In the maturation stage, the front and the vortex are superposed, and the atmosphere in the vortex is completely stable ($\theta_{ep} < 0$), making the deformation-related term increase the vertical vorticity but with a smaller magnitude.

From the above analysis, it can be concluded that the real effect of deformation on the vertical vorticity trend in fact takes place through the deformational frontogenesis process, but under the restriction of the baroclinic PV and the atmospheric stability. The inner physical process can be qualitatively analyzed from the MPV. Assuming the stability of the atmosphere (θ_{ep}) does not change during the deformational frontogenesis process, the increase of $|\nabla\theta_e|$ will thus make the inclination of the moist isentropic surfaces increase ($|\nabla\theta_e/\theta_{ep}|$). According to the expression of the vertical vorticity that is obtained from MPV [Eq. (3)],

$$\zeta = -\frac{P_m}{g\frac{\partial\theta_e}{\partial p}} + \frac{\boldsymbol{\zeta}_h\cdot\nabla\theta_e}{\frac{\partial\theta_e}{\partial p}} - f = -\frac{P_m}{g\frac{\partial\theta_e}{\partial p}} + |\theta_{ep}|\frac{\zeta_{h\theta_e}}{\theta_{ep}}\left|\frac{\nabla\theta_e}{\theta_{ep}}\right| - f\,, \tag{17}$$

the increase of the inclination of the isentropic surfaces will then induce the vertical vorticity development, as long as the atmosphere satisfies certain conditions ($\zeta_{h\theta_e}\theta_{ep} > 0$). In a certain sense, this is also part of the SVD theory, except that the factor (mainly deformation) that drives the isentropic surface inclination is considered.

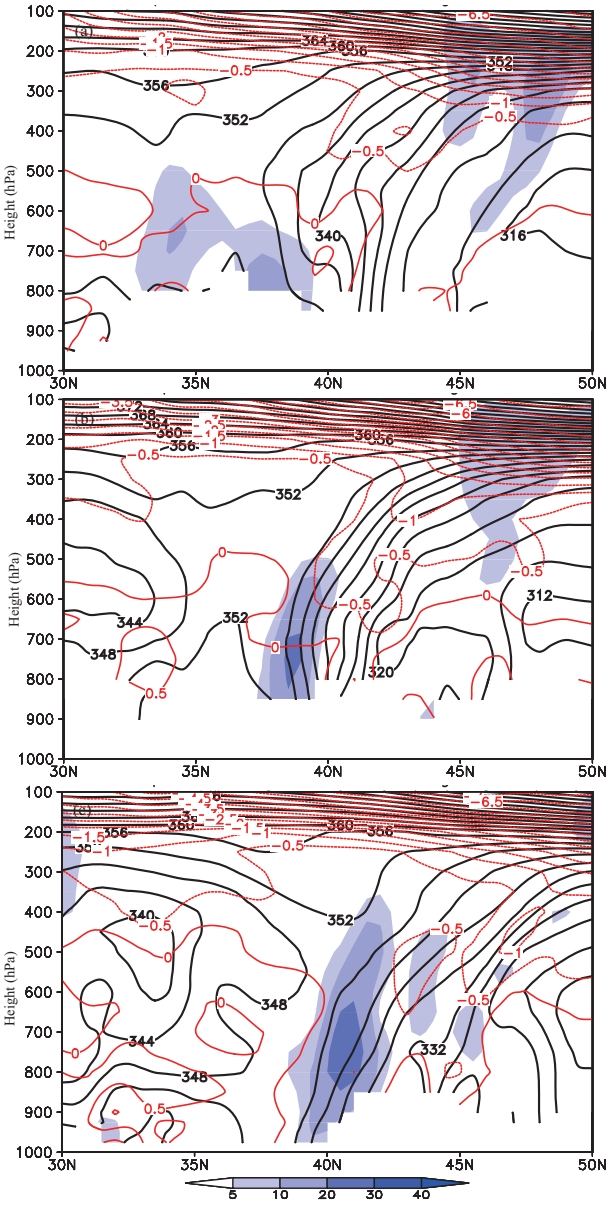

Fig. 10. Vertical distribution of θ_{ep} (red lines; units: 10^{-1} K hPa^{-1}) along the vortex center: (a) 105.5°E at 1200 UTC 20 July; (b) 109°E at 0000 UTC 21 July; (c) 116.5°E at 1200 UTC 21 July. The black solid lines are θ_e (units: K) contours, and the shaded areas are vertical vorticity (units: 10^{-5} s^{-1}).

4. Conclusion

A mathematical relation between deformation and vertical vorticity development is built by using the frontogenesis function as a substitute for the baroclinic variation term in the CVE, which is derived from the MPV. The relation provides valid evidence and diagnostics for the impact of deformation on mesoscale vortex development. Through the deformation-related term in the CVE, it is shown that the impact of deformation on increasing vertical vorticity not only relates to the deformation itself, but also needs the proper configuration of convective stability, moist baroclinicity and vertical wind shear. With this term, the impact of deformation on the development of a mesoscale vortex in a frontal heavy-rainfall case, which occurred during 20–22 July 2012, is diagnosed. The elements in this deformation-related term, including the deformation-induced baroclinic variation ($|E|\cos 2\gamma$), the convective stability (θ_{ep}) and the baroclinic part of MPV (P_{m2}), are diagnosed. The results show that, because the baroclinic MPV usually shows negative values in the vortex due to the influence of the front, and deformation often makes a positive contribution to the moist baroclinicity increase ($|E|\cos 2\gamma > 0$), whether or not deformation promotes the

vortex's development mostly depends on the stability of the baroclinic moist atmosphere. In the initial stage of the vortex, the atmosphere is convectively unstable, and deformation suppresses vortex development. In the development stage, as the cold front intrudes into the vortex, the stratification of the atmosphere in the vortex becomes stable above 750 hPa and remains unstable below 750 hPa, which causes the deformation to promote increasing vertical vorticity above 750 hPa and, thus, the vortex's development. In the maturation and dissipating stages, the stratifications in the vortex are all stable, and deformation promotes the vortex's development from its bottom to the top. By comparing the magnitudes of different terms in the CVE during the whole process of the vortex's evolution, it is in the vortex development stage that deformation shows a most significant impact on increasing vorticity. This is mostly due to a near-neutral level between a stable atmosphere and an unstable atmosphere, which makes the deformation-related term in the CVE much larger in the vortex development stage than in other stages.

Acknowledgements. This study was supported by a National Program on Key Basic Research project (Grant No. 2013CB 430105), the Key Program of the Chinese Academy of Sciences (Grant No. KZZD-EW-05), the National Key Technology Support Program (Grant No. 2015BAC03B04), the Special Scientific Research Fund of the Meteorological Public Welfare of the Ministry of Sciences and Technology (Grant No. GYHY200906004) and the National Natural Science Foundation of China (Grant Nos. 41175060, 41505040).

REFERENCES

Bishop, C. H., 1996a: Domain-independent attribution. Part I: Reconstructing the wind from estimates of vorticity and divergence using free space green's functions. *J. Atmos. Sci.*, **53**, 241–252.

Bishop, C. H., 1996b: Domain-Independent attribution. Part II: Its value in the verification of dynamical theories of frontal waves and frontogenesis. *J. Atmos. Sci.*, **53**, 253–262.

Bishop, C. H., and A. J. Thorpe, 1994a: Frontal wave stability during moist deformation frontogenesis. Part I: Linear wave dynamics. *J. Atmos. Sci.*, **51**(6), 852–873.

Bishop, C. H., and A. J. Thorpe, 1994b: Frontal wave stability during moist deformation frontogenesis. Part II: The suppression of nonlinear wave development. *J. Atmos. Sci.*, **51**(6), 874–888.

Bluestein, H. B., 1993: *Synoptic Dynamic Meteorology in Midlatitudes*. Oxford University Press, 594 pp.

Cai, M., 1992: A physical interpretation for the stability property of a localized disturbance in a deformation flow. *J. Atmos. Sci.*, **49**(23), 2177–2182.

Cai, M., and M. Mak, 1990: On the basic dynamics of regional cyclogenesis. *J. Atmos. Sci.*, **47**(12), 1417–1442.

Cui, X. P., G. X. Wu, and S. T. Gao, 2002: Numerical simulation and isentropic analysis of frontal cyclones over the western Atlantic Ocean. *Acta Meteorologica Sinica*, **60**(4), 385–399. (in Chinese)

Charney, J. G., 1947: The dynamics of long waves in a baroclinic westerly current. *J. Meteor.*, **4**, 136–162.

Davies, H. C., and J. C. Müller, 1988: Detailed description of deformation-induced semi-geostrophic frontogenesis. *Quart. J. Roy. Meteor. Soc.*, **114**, 1201–1219.

Deng, Q. H., 1986: The deformation field in the planetary boundary layer and heavy rainfall. *Journal of Academy of Meteorological Science*, **1**, 165–174. (in Chinese)

Eady, E. T., 1949: Long waves and cyclone waves. *Tellus*, **1**, 33–52.

Elhmaidi, D., A. Provenzale, T. Lili, and A. Babiano, 2004: Stability of two-dimensional vorticity filaments. *Physics Letters A*, **333**, 85–90.

Farrell, B. F., 1989: Transient development in confluent and diffluent flow. *J. Atmos. Sci.*, **46**, 3279–3288.

Gao, S. T., S. Yang, M. Xue, and C. M. Cui, 2008: Total deformation and its role in heavy precipitation events associated with deformation-dominant flow patterns. *Adv. Atmos. Sci.*, **25**(1), 11–28, doi: 10.1007/s00376-008-0011-y.

Holton, J. R., 2004: Circulation and vorticity. *An Introduction to Dynamic Meteorology*, Elsevier Academic Press, 84–114.

Hoskins, B. J., and F. P. Bretherton, 1972: Atmospheric frontogenesis models: Mathematical formulation and solution. *J. Atmos. Sci.*, **29**, 11–37.

Jiang, Y. Q., 2011: Study on the dynamic mechanism of formation of mesoscale weather systems triggered by wind perturbations. Ph.D dissertation, Nanjing University, 156 pp.

Jiang, Y. Q., Y. Wang, Z. G. Zhou, M. Lü, and J. Luo, 2011: Interaction index of vortex and deformation field. *Journal of PLA University of Science and Technology (Natural Science Edition)*, **12**(6), 685–689. (in Chinese)

Keyser, D., and R. A. Anthes, 1982: The influence of planetary boundary layer physics on frontal structure in the Hoskins-Bretherton horizontal shear model. *J. Atmos. Sci.*, **39**, 1783–1802.

Keyser, D., M. J. Reeder, and R. J. Reed, 1988: A Generalization of Petterssen's Frontogenesis Function and Its Relation to the Forcing of Vertical Motion. *Mon. Wea. Rev.*, **116**, 762–781.

Kuo, H. L., 1949: Dynamics instability of two-dimensional nondivergent flow in a barotropic atmosphere. *J. Meteor.*, **6**, 105–122.

Li, Y., L. S. Chen, and X. T. Lei, 2005: Moisture potential vorticity analysis on the extratropical transition processes of Winnie (1997) and Bilis (2000). *Journal of Tropical Meteorology*, **21**(2), 142–152. (in Chinese)

Mak, M., 1991: Dynamics of an atmospheric blocking as deduced from its local energetics. *Quart. J. Roy. Meteor. Soc.*, **117**, 477–493.

Mak, M., and M. Cai, 1989: Local barotropic instability. *J. Atmos. Sci.*, **46**, 3289–3311.

Meng, W. G., A. Y. Wang, J. N. Li, R. Q. Feng, and E. B. Hou, 2004: Moist potential vorticity analysis of the heavy rainfall and mesoscale convective systems in South China. *Chinese J. Atmos. Sci*., **28**(3), 330–341. (in Chinese)

Moon, Y., and D. S. Nolan, 2015: Spiral rainbands in a numerical simulation of Hurricane Bill (2009). Part II: Propagation of inner rainbands. *J. Atmos. Sci.*, **72**, 191–215.

Petterssen, S., 1956: *Weather Analysis and Forecasting Vol. I: Motion and Motion Systems*. McGraw-Hill, 428 pp.

Renfrew, I. A., A. J. Thorpe, and C. H. Bishop, 1997: The role of the environmental flow in the development of secondary frontal cyclones. *J. Atmos. Sci.*, **123**, 1653–1675.

Rivière, G., and A. Joly, 2006a: Role of the low-frequency deformation field on the explosive growth of extratropical cyclones

at the jet exit. Part I: Barotropic critical region. *J. Atmos. Sci.*, **63**, 1965–1981.

Rivière, G., and A. Joly, 2006b: Role of the low-frequency deformation field on the explosive growth of extratropical cyclones at the jet exit. Part II: Baroclinic critical region. *J. Atmos. Sci.*, **63**, 1982–2006.

Rozoff, C. M., W. H. Schubert, B. D. McNoldy, and J. P. Kossin, 2006: Rapid filamentation zones in intense tropical cyclones. *J. Atmos. Sci.*, **63**, 325–340.

Shutts, G. J., 1983: The propagation of eddies in diffluent jetstreams: Eddy vorticity forcing of "blocking" flow fields. *Quart. J. Roy. Meteor. Soc.*, **109**, 737–761.

Spensberger, C., and T. Spengler, 2014: A new look at deformation as a diagnostic for large-scale flow. *J. Atmos. Sci.*, **71**, 4221–4234.

Thomas, L. N., 2012: On the effects of frontogenetic strain on symmetric instability and inertia-gravity waves. *J. Fluid Mech.*, **711**, 620–640.

Wang, J. Z., S. F. Ma, and Y. H. Ding, 1996: Application of potential vorticity theory to analysis of formative mechanism of torrential rain. *Quarterly Journal of Applied Meteorology*, **7**, 19–27.

Wang, X. B., and R. S. Wu, 2001: The development of symmetric disturbance superposed on baroclinic frontal zone under the action of deformation field. *Acta Meteorologica Sinica*, **15**(4), 420–435.

Wang, Y. Q., 2008: Rapid filamentation zone in a numerically simulated tropical cyclone. *J. Atmos. Sci.*, **65**, 1158–1181.

Wang, Z. Q., W. J. Zhu, and A. M. Duan, 2010: A case study of snowstorm in Tibetan Plateau induced by Bay of Bengal storm: Based on the theory of slantwise vorticity development. *Plateau Meteorology*, **29**(3), 703–711. (in Chinese)

Weiss, J., 1991: The dynamics of enstrophy transfer in two-dimensional hydrodynamics. *Physica D: Nonlinear Phenomena*, **48**, 273–294.

Whitaker, J. S., and R. M. Dole, 1995: Organization of storm tracks in zonally varying flows. *J. Atmos. Sci.*, **52**(8), 1178–1191.

Wu, G. X., 2001: Comparison between the complete-form vorticity equation and the traditional vorticity equation. *Acta Meteorologica Sinica*, **59**(4), 385–392. (in Chinese)

Wu, G. X., and Y. P. Cai, 1997: Vertical wind shear and downsliding slantwise vorticity development. *Scientia Atmospherica Sinica*, **21**(3), 273–282. (in Chinese)

Wu, G. X., and H. Z. Liu, 1999: Complete form of vertical vorticity tendency equation and slantwise vorticity development. *Acta Meteorologica*, **57**(1), 1–15. (in Chinese)

Wu, G. X., Y. P. Cai, and X. J. Tang, 1995: Moist potential vorticity and slantwise vorticity development. *Acta Meteorologica Sinica*, **53**(4), 387–405. (in Chinese)

Wu, G. X., Y. J. Zheng, and Y. M. Liu, 2013: Dynamical and thermal problems in vortex development and movement. Part II: Generalized slantwise vorticity development. *Acta Meteorologica Sinica*, **27**(1), 15–25.

Yang, S., S. T. Gao, and C. G. Lu, 2014: A generalized frontogenesis function and its application. *Adv. Atmos. Sci.*, **31**(5), 1065–1078, doi: 10.1007/s00376-014-3228-y.

Yang, S., S. T. Gao, and C. G. Lu, 2015: Investigation of the Meiyu front using a new deformation frontogenesis function. *Adv. Atmos. Sci.*, **32**(5), 635–647, doi: 10.1007/s00376-014-4147-7.

Yu, H., and G. X. Wu, 2001: Moist baroclinicity and abrupt intensity change of tropical cyclone. *Acta Meteorologica Sinica*, **59**(4), 440–449 (in Chinese).

Zheng, Y. J., G. X. Wu, and Y. M. Liu, 2013: Dynamical and thermal problems in vortex development and movement. Part I: A PV-Q view. *Acta Meteorologica Sinica*, **27**(**??**), 1–14.